New limit on the strength of mixing between ν_μ and ν_e

L. A. Ahrens, S. H. Aronson, P. L. Connolly,* B. G. Gibbard, M. J. Murtagh, S. Murtagh, S. Terada,† and D. H. White
Physics Department, Brookhaven National Laboratory, Upton, New York 11973

J. L. Callas, D. Cutts, J. S. Hoftun, R. E. Lanou, and T. Shinkawa†
Department of Physics, Brown University, Providence, Rhode Island 02912

K. Amako and S. Kabe
National Laboratory for High Energy Physics (KEK), Ibaraki-Ken 305, Japan

Y. Nagashima, Y. Suzuki, and S. Tatsumi
Physics Department, Osaka University, Toyanaka, Osaka 560, Japan

K. Abe,† E. W. Beier, D. C. Doughty, L. S. Durkin, S. M. Heagy, M. Hurley, A. K. Mann, F. M. Newcomer, H. H. Williams, and T. York
Department of Physics, University of Pennsylvania, Philadelphia, Pennsylvania 19104

D. Hedin, M. D. Marx, and E. Stern
Department of Physics, State University of New York, Stony Brook, New York 11794
(Received 23 October 1984)

Measurements have been made of the reactions $\nu_e n \to e^- p$ and $\nu_\mu n \to \mu^- p$ in a detector located an effective distance of 96 m from a neutrino source. These measurements yield directly the energy-dependent ratio of the neutrino fluxes $[\Phi(E(\nu_e))/\Phi(E(\nu_\mu))]_{\text{obs}}$ incident on the detector. When combined with an estimate of the flux ratio emanating from the source $[\Phi(E(\nu_e))/\Phi(E(\nu_\mu))]_{\text{calc}}$, the measured ratio provides an upper limit on the strength of mixing between ν_μ and ν_e. We obtain $\sin^2 2\alpha < 3.4\times 10^{-3}$ (90% C.L.) in the limit of large mass difference Δm^2 ($\equiv |m_1{}^2 - m_2{}^2|$) between neutrino mass eigenstates, m_1 and m_2; and an upper limit on the product $\Delta m^2 \sin 2\alpha < 0.43$ eV^2 in the limit of small mass difference.

If the masses of neutrinos are nondegenerate, and if separate lepton number is not exactly conserved, neutrinos of a given flavor will oscillate into neutrinos of another flavor.[1] In this paper we report measurements of events from the reactions $\nu_e n \to e^- p$ and $\nu_\mu n \to \mu^- p$ induced in a neutrino detector by wide-band neutrino fluxes $\Phi(E(\nu_e))$ and $\Phi(E(\nu_\mu))$, respectively. The measurements yield directly the flux ratio

$$[\Phi(E(\nu_e))/\Phi(E(\nu_\mu))]_{\text{obs}}$$

incident on the detector. After subtraction of the estimated flux ratio

$$[\Phi(E(\nu_e))/\Phi(E(\nu_\mu))]_{\text{calc}}$$

initially present in the beam, no evidence for the oscillation $\nu_\mu \to \nu_e$ is present. The data exclude a significant region of the Δm^2-$\sin^2 2\alpha$ space,[2] where $\Delta m^2 = |m_1{}^2 - m_2{}^2|$ in eV^2, m_1 and m_2 are neutrino mass eigenstates, and $\sin^2 2\alpha$ is the strength of mixing between ν_μ and ν_e.

The neutrino detector consists of 112 planes of liquid scintillator (each plane 4 m$\times$4 m in area $\times$8 cm thick) and 224 planes of proportional drift cells (4.2 m$\times$4.2 m in area $\times$3.8 cm thick) uniformally interspersed. The fine segmentation (1792 scintillator cells and 12 096 proportional drift cells) and the pulse-height and timing characteristics of the elements provide determination of event topology, identification of electromagnetic showers, and substantial discrimination through dE/dx measurements between electrons and photons as well as pions and protons. Immediately downstream of the detector is a 30-ton shower counter of area 4 m$\times$4 m with 12 radiation lengths to provide additional containment of showers from events occurring at the downstream end of the detector. Further downstream is a magnet of aperture 1.8 m$\times$1.8 m$\times$0.46 m for study of the very-low-q^2 region of the ν_μ-induced quasielastic reaction and measurement of the antineutrino contamination present in the incident neutrino beam.

The detector was designed specifically to measure the elastic-scattering reactions $\nu_\mu(\bar{\nu}_\mu)e \to \nu_\mu(\bar{\nu}_\mu)e$ and $\nu_\mu(\bar{\nu}_\mu)p \to \nu_\mu(\bar{\nu}_\mu)p$ and quasielastic reactions $\nu_\mu n \to \mu^- p$ and $\bar{\nu}_\mu p \to \mu^+ n$, and was therefore well suited to the measurement of $\nu_e n \to e^- p$. The data described here are part of a data sample obtained in a single exposure of 0.88×10^{19} protons on the target from which neutrinos are produced at the Brookhaven Alternating Gradient Synchrotron (AGS). Data from the same run were used to

determine the cross section for the reaction $\nu_\mu e^- \rightarrow \nu_\mu e^-$, which was presented in an earlier report that also provided a brief description of the apparatus.[3]

Two data sets are employed in the present measurement: (i) e^-p-final-state data and (ii) μ^-p-final-state data. In data set (i) the electron angle and electron energy are measured and no requirement (apart from a limit on range) is placed on, or direct use made of, the recoil proton. In data set (ii) the proton angle and proton kinetic energy are measured, but no information relating to the outgoing muon is used apart from its clear presence. Taking into account the lower-q^2 region and larger fiducial volume from which the e^-p data were obtained, the acceptance for e^-p events was approximately 10 times greater than that for μ^-p events. In addition, the e^-p data were extracted from the entire exposure of 0.88×10^{19} protons on target, while the μ^-p data were selected uniformly from the entire run but with an equivalent exposure of 0.14×10^{19} protons on target. These factors combined to make possible the measurement of a flux ratio $\phi(E(\nu_e))/\phi(E(\nu_\mu))$ in the vicinity of 1 GeV of order of magnitude 10^{-3}.

To obtain e^-p events raw data coming from 1.25×10^6 AGS beam bursts were processed through a coarse computer-based filter program[3] designed to remove events not containing a single electromagnetic shower within the angular interval $\theta_e < 240$ mrad relative to the mean neutrino beam direction. The resulting sample was scanned by physicists to eliminate events which the filter did not remove such as some with more than one electromagnetic shower or with an interacting hadron. Events exhibiting an electromagnetic shower with an associated upstream vertex were set aside for use as a control sample of photons.

The shower angle was measured by a fit to all shower hits in the proportional drift cells, and the shower energy was found by summing the deposited energy in the calorimeter cells with a correction for invisible energy of approximately 40%. These methods gave an angular resolution of $\Delta\theta = 30$ mrad, and an energy resolution

$$\Delta E/E = 0.12/\sqrt{E}\ (\text{GeV})\ .$$

After requiring that $0.21 < E_e \leq 5.1$ GeV, 873 shower events remained in the fiducial region.

There are three categories of background processes that produce forward electromagnetic showers: (a) production of π^0 by ν_μ-induced neutral-current processes ($\nu_\mu p\pi^0$, $\nu_\mu n\pi^0$), (b) inelastic processes from ν_e ($e^-p\pi^+$, $e^-n\pi^+$, $e^-p\pi^0$), and (c) the interaction $\nu_\mu e \rightarrow \nu_\mu e$. Reactions with a π^+ in the final state were recognized by the delayed signal from the π-μ-e decay chain. In Fig. 1(a) is shown the shower energy distribution of all events retained after subtraction of the π^+ background events. Most photon-induced showers from $\nu_\mu p\pi^0$ and $\nu_\mu n\pi^0$ were recognized by their association with a significant deposition of energy or a vertex upstream of the shower. In Fig. 1(b) is the energy distribution of the photon-induced showers in the control sample. We expect from calculation and observation[3] the e^-p candidate sample below 0.9 GeV [Fig. 1(a)] to contain mostly photons with a small number of electrons from $\nu_\mu e \rightarrow \nu_\mu e$, and only very few electrons from $\nu_e n \rightarrow e^- p$ because of the 240-mrad criterion. Hence it is possible to subtract the photon-induced events above 0.9 GeV in Fig. 1(a) by normalizing the distributions in Figs. 1(a) and 1(b) below 0.9 GeV.

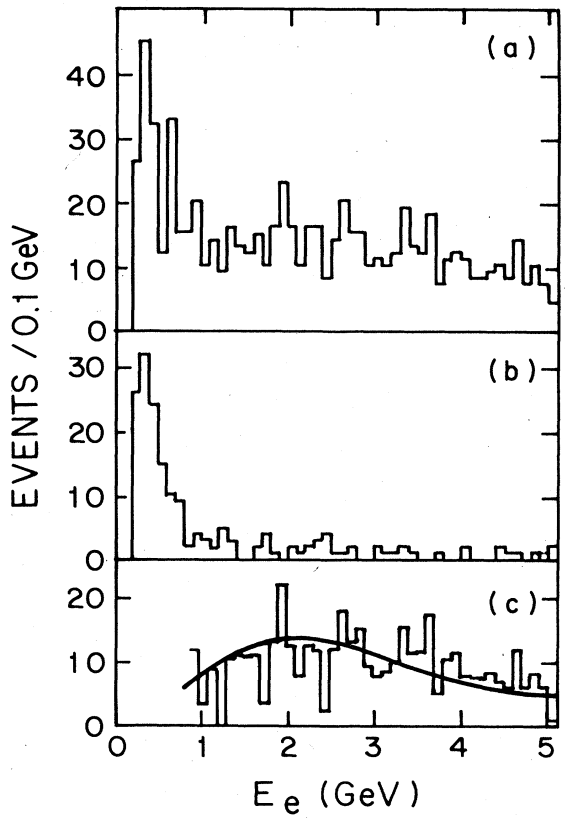

FIG. 1. (a) Shower energy distribution of all possible $\nu_e n \rightarrow e^- p$ candidate events. (b) Shower energy distribution of photons recognized as emanating from an upstream event vertex. (c) The resulting e^-p energy distribution after all background subtractions. The solid curve is the Monte Carlo calculated energy distribution of e^- from $\nu_e n \rightarrow e^- p$.

There were initially 653 events in the sample with $E_e > 0.9$ GeV of which 20% were removed by a bin-by-bin subtraction of the π^+ events; 13% of the remaining events were removed bin-by-bin using the distribution in Fig. 1(b). Further subtractions were made of the fraction of $\nu_\mu e$ events[3] (5.8%), and of energetic ($e^-p\pi^0$) events which by calculation amounted to 3%. The final e^-p sample contains 418 events in the region $0.9 < E_e < 5.1$ GeV; it is shown in Fig. 1(c) where comparison is made with the result of a Monte Carlo calculation.

Each event in data set (ii) was initially selected as a two-prong event capable of reconstruction by a track fitting program. It was then required that one of the prongs be identified by range and ionization[4] as a proton while the other prong was required to exit the detector. The background in this data set when acceptance criteria were applied consisted of charged-current single-π^+ production (13% of the observed $\nu_\mu n \rightarrow \mu^- p$ rate) plus a small contribution ($\sim$3%) from single-π^0 and multipion events. Reactions with a π^+ were corrected for empirically by the

π-μ-e decay chain as described above. The π^0 and multipion components were estimated by Monte Carlo calculation. The final $\mu^- p$ sample contains 1370 events.

The neutrino spectra $\Phi(E(\nu_\mu))$ and $\Phi(E(\nu_e))$ were obtained from data sets (i) and (ii) using Monte Carlo–calculated event acceptance functions $a^{\mu p}(E)$ and $a^{ep}(E)$, the known magnitude and energy dependence of the quasielastic cross section[5] $\sigma_{\rm QE}(E)$, and the measured number of protons on target ($N_{\rm POT}$); viz.,

$$\Phi(E(\nu_l))=\frac{(\text{No. of observed QE events between } E \text{ and } E+\Delta E)}{[\sigma_{\rm QE}(E)a^{lp}(E)\Delta E\, N_{\rm POT}\times(\text{No. of target neutrons})]} \tag{1}$$

in $\nu_l/[\text{GeV m}^{-2}(10^{13}N_{\rm POT})]$, where $l=e$ or μ. The resulting spectra are shown in Figs. 2(a) and 2(b).

To test, albeit indirectly, the calculation that provided $a^{lp}(E)$, the only nonempirical quantity in Eq. (1), the Q^2 distributions for the $\mu^- p$ and $e^- p$ samples were constructed and compared with the expected theoretical distribution.[5] The results are shown in Fig. 3, where the scale of the vertical axis is given in arbitrary units because the absolute value has been assumed implicitly through $\sigma_{\rm QE}(E)$ in Eq. (1). The satisfactory agreement exhibited in Fig. 3 demonstrates that the acceptance functions $a^{ep}(E_\nu,Q^2)$ and $a^{\mu p}(E_\nu,Q^2)$, when taken over all E_ν and applied to the data, yield the correct Q^2 distributions within experimental error.

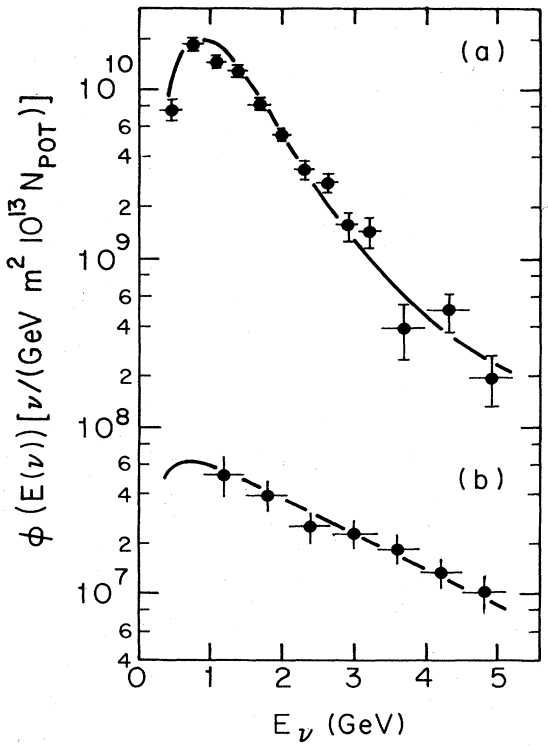

FIG. 2. (a) $\Phi(E(\nu_\mu))$ obtained from data set (i) of $\nu_\mu n\to\mu^- p$ events. (b) $\Phi(E(\nu_e))$ obtained from data set (ii) of $\nu_e n\to e^- p$ events. The solid curves are calculated from a neutrino beam program (Ref. 7). Errors shown are statistical only. The experimental resolution in E_ν is dominated by Fermi motion of the nucleon in the target nucleus and is roughly $\pm 25\%$ at $E_\nu=1$ GeV.

It follows from this expression above for $\Phi(E(\nu_l))$ that the flux ratio $\Phi(E(\nu_e))/\Phi(E(\nu_\mu))$ is given simply by the ratio of the corrected numbers of $e^- p$ and $\mu^- p$ events since the data were taken at the same time in the same beam. That ratio is shown as a function of energy in Fig. 4(a). The systematic error on the points in Fig. 4(a) (not included in the error bars) is the result of uncertainty in the calculated ratio

$$\sigma_{\rm QE}(E)a^{\mu p}(E)/\sigma_{\rm QE}(E)a^{ep}(E)$$

due to the difference of the q^2 regions occupied by the two data sets (see Fig. 3). By varying input parameters in the ratio calculation, the systematic error was determined to be less than $\pm 14\%$. Note that it is the ratio $\Phi(E(\nu_e))/\Phi(E(\nu_\mu))$ which must be determined reliably since it alone is salient to the extraction of the neutrino oscillation parameters.

If it is supposed that all of the ν_e are the result of oscillations of the type $\nu_\mu\to\nu_e$, upper limits on the mixing angle and Δm^2 can be set directly from the data in Fig. 4(a). In the limit of large Δm^2, i.e., short oscillation wavelength ($4\pi E_\nu/\Delta m^2 \ll L$, the neutrino source to detector distance, in meters), the oscillation probability

$$P(\nu_\mu\to\nu_e)=\sin^2 2\alpha\,\sin^2[1.27(L/E_\nu)\Delta m^2]$$

becomes

$$P(\nu_\mu\to\nu_e)=\tfrac{1}{2}\sin^2 2\alpha\ ,$$

independent of L/E_ν, where α is the angle of mixing be-

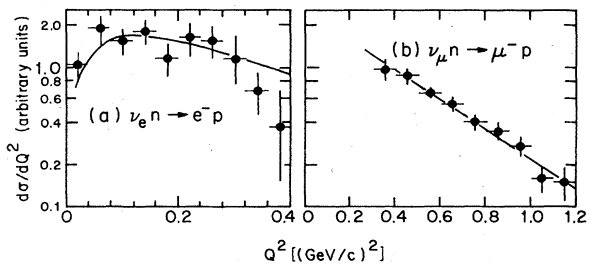

FIG. 3. The Q^2 distributions (a) $\nu_e n\to e^- p$ and (b) $\nu_\mu n\to\mu^- p$ constructed from the fully corrected data of sets (i) and (ii) compared with the theoretical distribution ($M_A=1.05$). The vertical scale is in arbitrary units because $\sigma_{\rm QE}(E)$ has been assumed in extracting the spectra of Fig. 2.

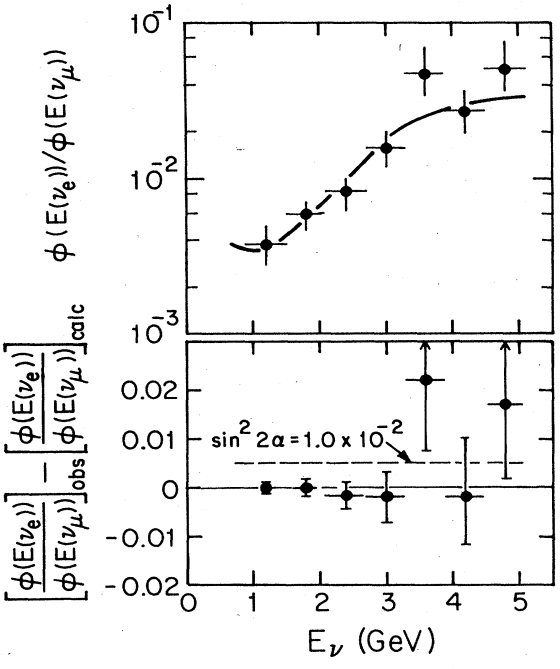

FIG. 4. (a) Plot of the flux ratio $\Phi(E(\nu_e))/\Phi(E(\nu_\mu))$ against E_ν. The points represent the data while the solid curve is calculated from a neutrino beam program (Ref. 7). (b) Plot of the difference between the observed and calculated flux ratios against E_ν. The dashed line is the limit on $\sin^2 2\alpha$ obtained without subtraction (see text).

tween ν_μ and ν_e, and E_ν is the neutrino energy in MeV. One finds, at 90% confidence level, using the data between 0.9 and 1.5 GeV in Fig. 4(a),

$$\sin^2 2\alpha \leq 1.0\times 10^{-2} .$$

In the limit of small Δm^2 or very long oscillation wavelength,

$$P(\nu_\mu \rightarrow \nu_e) = \sin^2 2\alpha [1.27(L/E_\nu)\Delta m^2]^2 ,$$

from which is obtained at 90% confidence level,

$$\Delta m^2 \sin 2\alpha \leq 0.67 \text{ eV}^2 ,$$

for the properly weighted neutrino energy, roughly 1200 MeV, and $L=96$ m, the condition of this experiment.[6]

The limits above may be improved if the number of ν_e in the incident neutrino beam (due to the decays of muons and kaons) relative to the number of ν_μ in the incident beam can be estimated as a function of energy with reasonable accuracy and subtracted from the observed values

$$[\Phi(E(\nu_e))/\Phi(E(\nu_\mu))]_{obs}$$

in Fig. 4(a). We have used a neutrino beam program[7] to do this with the results shown as the solid lines in Figs. 2 and 4(a). The agreement between the observed and calculated ν_μ and ν_e spectra in Fig. 2 is a confirmation of the validity of the beam program and of the parameters of pion and kaon production that are input to it. We emphasize again, however, that it is only the ratio

$$[\Phi(E(\nu_e))/\Phi(E(\nu_\mu))]_{calc}$$

shown as the solid line in Fig. 4(a) that needs to be calculated accurately.

The shape of $\Phi(E(\nu_e))/\Phi(E(\nu_\mu))$ can be understood from Table I, which gives as a function of energy the fraction of $\Phi(E(\nu_e))$ and the fraction of $\Phi(E(\nu_\mu))$ that arise from pions and from kaons relative to the total $\Phi(E(\nu_e))$ and total $\Phi(E(\nu_\mu))$. One sees also from Table I that the uncertainty in

$$[\Phi(E(\nu_e))/\Phi(E(\nu_\mu))]_{calc}$$

due to uncertainty in the K/π ratio—the sole input that quantitatively affects the flux ratio—does not exceed 15% at any neutrino energy between 1 and 5 GeV, when 20% variations are assumed in the yield of either pions or kaons.

More importantly, Table I shows that at $E_\nu=1$ GeV two-thirds of $\Phi(E(\nu_e))$ and 99% of $\Phi(E(\nu_\mu))$ result from the π-μ-e decay chain alone. At $E_\nu=5$ GeV, the pion and kaon roles are essentially reversed. This accounts for the relatively small variations in $\Phi(E(\nu_e))/\Phi(E(\nu_\mu))$ in the vicinity of those energies as the K/π ratio is varied. Furthermore, in the large Δm^2 limit, the ratio $\Phi(E(\nu_e))/\Phi(E(\nu_\mu))$ is independent of L/E as we have seen, and consequently the contribution from oscillations at any energy in Fig. 4(a) cannot be larger than that given by the data point near 1 GeV. Hence the data at the higher energies in Fig. 4(a) serve as a direct test within experimental error of the accuracy of the calculation of $\Phi(E(\nu_e))/\Phi(E(\nu_\mu))$.

The result of the subtraction is shown in Fig. 4(b) in which is plotted the difference between $[\Phi(E(\nu_e))/\Phi(E(\nu_\mu))]_{obs}$ and $[\Phi(E(\nu_e))/\Phi(E(\nu_\mu))]_{calc}$ as a function of E_ν. The errors shown on the data points include a systematic uncertainty of 20% [comprised of equal contributions from the acceptance functions $a^{lp}(E)$ and the flux calculation] in quadrature with the statistical uncertainties. It is clear that no evidence for the oscillation $\nu_\mu \rightarrow \nu_e$ is present in Fig. 4(b). Using the data between 900 and 2100 MeV, the region in the Δm^2-$\sin^2 2\alpha$ space excluded with 90% confidence is shown in Fig. 5 from which one

TABLE I. An example of the relative kaon contributions $R_e^K \equiv \Phi(\nu_e(K))/\Phi(\nu_e(\text{all}))$ and $R_\mu^K \equiv \Phi(\nu_\mu(K))/\Phi(\nu_\mu(\text{all}))$ to the total fluxes $\Phi(E(\nu_e))$ and $\Phi(E(\nu_\mu))$, respectively, is given in the second and third columns. Relative pion contributions are $(1-R_e^K)$ and $(1-R_\mu^K)$. The last two columns exhibit the variation in $\Phi(E(\nu_e))/\Phi(E(\nu_\mu)) = [1-R_e^K(1-r)]/[1-R_\mu^K(1-r)]$ for 20% changes in the value of r, the ratio of the kaon to pion yields integrated over contributing meson momenta. The normalization is arranged to give $\Phi(E(\nu_e))/\Phi(E(\nu_\mu))=1.00$ for $r=1.0$.

Energy (GeV)	$\Phi(E(\nu_e))/\Phi(E(\nu_\mu))$ R_e^K	R_μ^K	$r=1.2$	$r=0.8$
1	0.34	0.006	1.07	0.94
2	0.68	0.013	1.113	0.89
3	0.85	0.10	1.15	0.87
4	0.90	0.36	1.10	0.90
5	0.94	0.67	1.05	0.95

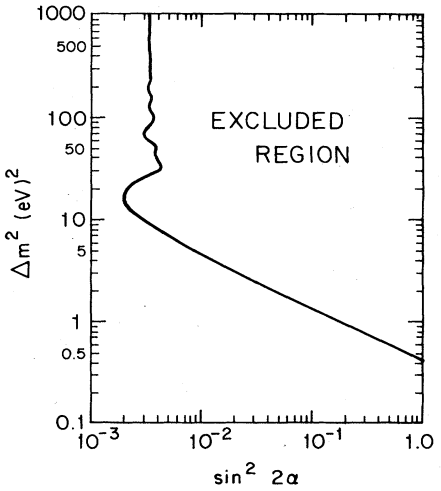

FIG. 5. The region of the Δm^2-$\sin^2 2\alpha$ space excluded with 90% confidence by this experiment.

obtains

$\sin^2 2\alpha \leq 3.4\times 10^{-3}$ at 90% C.L. ,

in the large-Δm^2 limit

and

$\Delta m^2 \sin 2\alpha \leq 0.43$ eV^2 at 90% C.L. ,

in the small-Δm^2 limit .

These limits extend the excluded region of the Δm^2-$\sin^2 2\alpha$ space beyond that of the previous best search[9] for $\nu_\mu \rightarrow \nu_e$. They are based on a comparison of the neutrino flux ratio as a function of neutrino energy obtained from measurements of quasielastic events with the neutrino flux ratio as a function of neutrino energy calculated semiempirically to emanate from a neutrino source. This procedure has, in addition to simplicity, the merit that it delineates possible systematic errors in the limits determined from it and allows them to be estimated accurately.

We wish to thank R. R. Rau and N. P. Samios of the Brookhaven National Laboratory for their encouragement and the staff of the AGS and the Brookhaven Physics Department for their cooperation. We also wish to thank Roger D. Carlini for his work on the neutrino beam program and the technical assistance personnel at the respective universities for their excellent and untiring support. This work was supported in part by the U. S. Department of Energy, the Japanese Ministry of Education, Science and Culture through the Japan-U.S.A. Cooperative Research Project on High Energy Physics, the U. S. National Science Foundation, and the Stony Brook Incentive Fund.

---

*Deceased.

†Now at KEK, Ibaraki-Ken 305, Japan.

[1]For reviews of neutrino oscillations, see, e.g., A. K. Mann and H. Primakoff, Phys. Rev. D **15**, 655 (1977); S. M. Bilenky and B. Pontecorvo, Phys. Rep. **41**, 225 (1978).

[2]For a recent summary of the status of neutrino mass and mixing experiments, see M. H. Shaevitz, in *Proceedings of the 1983 International Symposium on Lepton and Photon Interactions at High Energies, Ithaca, New York,* edited by D. G. Cassel and D. L. Kreinick (Newman Laboratory of Nuclear Studies, Cornell University, Ithaca, 1983), p. 132.

[3]L. A. Ahrens *et al.*, Phys. Rev. Lett. **51**, 1514 (1983); **54**, 18 (1985).

[4]D. C. Doughty, Jr., Ph.D. thesis, University of Pennsylvania, 1984.

[5]N. J. Baker *et al.*, Phys. Rev. D **23**, 2499 (1981).

[6]The effective neutrino source to detector distance is calculated as follows. The distance from the target on which protons from the AGS impinge to the end of the meson decay region is 61.7 m, along which meson decays occur almost uniformly. The distance from the end of the decay region to the middle of the detector is 65.6 m. Hence adding one-half the length of the decay region to 65.6 m yields 96.4 m.

[7]The beam program used was a CERN wide-band program (Hydra Applications Library, NUBEAM, C. Visser, CERN, 1979) modified extensively by R. D. Carlini, Los Alamos National Laboratory. The systematics of pion and kaon production used to obtain the curves in Figs. 2 and 4(a) were based on the semiempirical studies cited in Ref. 8. The two studies give for r, the K^+/π^+ ratio averaged over all meson momenta from 1 to 14 GeV/c, 0.083 (GHR), and 0.089 (SW). In either study variations in the ratio $\phi(E(\nu_e))/\phi(E(\nu_\mu))$ at any E_ν between 1 and 5 due to $\pm 20\%$ variations in r differ by less than 15% from the values of $\phi(E(\nu_e))/\phi(E(\nu_\mu))$ that obtain for r at its central value in that study (see Table I). Details of this work on neutrino beams at BNL are in D. H. White, Report No. BNL-OG793 (unpublished) and will be published elsewhere.

[8]J. R. Sanford and C. L. Wang, Report No. BNL 11479, 1967 (unpublished); H. Grote, R. Hagedorn, and J. Ranft, CERN report, 1979 (unpublished).

[9]N. J. Baker *et al.*, Phys. Rev. Lett. **47**, 1576 (1981).